Air/ liquid interface for homogenous Dispersion of MoS_2 nanosheets in polyindole matrix assisted by Langmuir Technique

5.1 Introduction

Advent of new era of materials science is manifested by unearthing of nanomaterials with applications in electronics, sensors, electrocatalysis, optoelectronics, bio related applications field, etc. [21,131,132]. These nano sized materials allow us to tailor their physical properties by varying experimental conditions, thus enabling their applicability in various fields. Further, it is conducive to employ rather green synthesis protocols for these nanostructures utilizing environmental friendly precursors and medium [131, 133]. Among the nanomaterials, 2D layered materials (graphene and its analogues, like transition metal dichalcogenides) have grabbed greater attention due to their distinctive material properties and their applicability in sensors, electronics, catalysis, energy-storage and optoelectronic fields [134-136]. Among transition dichalcogenides, molybdenum disulfide (MoS_2) displays highest conductivity and has relieved much from the scalability and economic issues to a large extent [135,136]. Various reported synthetic procedures for MoS_2 are micromechanical exfoliation, liquid phase exfoliation, physical vapor deposition, chemical solution process, chemical vapor deposition, etc. that require severe experimental conditions, but hydrothermal route (solution-based process) offers best control over MoS_2 nanosheet morphology in mild condition with maximum exfoliation in liquid phase [136-140]. MoS_2 in bulk state is a 3 atoms (S-Mo-S) layered structure stacked via van der Waals interactions, those need to be intervened in order to exploit its few layers intrinsic properties either by exfoliating chemically or physically [137,140]. MoS_2 nanosheets with minimal interference from the counter ions synthesized

via hydrothermal route are generally few layered, that need to be exfoliated or dispersed in proper dispersion medium to avoid the risk of re-stacking [136,137]. Coleman et al. has demonstrated exfoliation via sonication in non-volatile organic solvents (non-ecofriendly) to obtain single or a few layered nanosheets of MoS_2, but the organic wrapping layers blocked its scope for usage in further applications [137]. Later, Zhang and coworkers, reported the exfoliation of MoS_2 in an ethanol-water mixture that could be removed easily later [135]. Usually, solvent assisted exfoliation weakens the interlayer interaction and enables the intercalation of small ions or molecules within the layers that can be removed later. Thus, dispersion medium and matrix play a significant role in controlling the extent of exfoliation for appropriate application.

There have been many attempts to blend various polymers or form composite with other materials inorder to obtain desired properties [135,136]. Similarily, MoS_2 (possesing large surface area, high electrical conductivity, and heterogeneous electron transfer properties) when reinforced with various polymers have significantly enhanced composite's thermal, mechanical and electrical properties synergistically [135, 138]. But the high cost, low productivity and poor fabricating techniques have limited their merits [135,137]. Recently, Tang et al. have prepared polypyrrole-MoS_2 nanocomposite via controlled polymerization of the monomer adsorbed on MoS_2 sheets (exfoliated via lithium ion) [138]. Here, we have adopted hydrothermal route directly yielding nanosheet morphology, that are later exfoliated in ethanol-water mixture in the presence of monomer (indole) discarding the usage of other intercalating agent. The reason for interest in polyindole (PIn) among the most studied conducting polymers, is their excellent thermal stability, high redox activity, fast electrochromic response and better environmental stability with their prominence in sensors, electrocatalysis, electrochromic

devices, energy storage, biosensor domains till date [51,55,69,72,76,119,141]. Besides all these, poor electrical conductivity of PIn relative to Sulfur containing polymers with alkyl chain like Poly (3-alkylthiophene) (P3-AT), diminishes PIn family significance in organic electronics [56,57,64,76,129]. In the past few decades, remarkable enhancement in redox and electrical properties of PIn family has been dealt via composites formation with CNT, graphene,etc. various conducting materials [69]. Nevertheless, high cost, poor synthetic yield and failure in large area film formation of these materials reduce their industrial implication. These above issues still demand a simple, environmently benign and good synthetic yield protocols for PIn composite formation to enhance their film stability and conductivity. The major hurdle in their usage in electronic devices is their lack in formation of thin flexible films due to their poor solution processability in pure form (no surfactant). Solution processability issue has been already addressed in our previous report that clearly explains the formation of thin film of PIn via Langmuir-Blodgett (LB) method [76]. Though the report states the stable film formation of PIn at air-water interface, their uniformity for multiple layers deposition onto substrates can be improved by varying the substrate nature and lifting style employing Langmuir-Schaefer (LS) method. Some previous reports have also preferred LS method for non-amphiphilic films like polymers as it minimizes the disruptive force disturbing the uniformity of rigid monolayer during vertical upliftment [53,54]. Herein, we have employed LS method for film fabrication and maximum interfacial interaction between MoS_2 and the dispersion matrix (PIn) at molecular level. Previously reported results promoted the addition of surfactants to MoS_2 nanosheets to prevent their sinking in the trough and to polymers to aid their processability and orientation alongwith compromise with their intrinsic electrical properties [53,54,76]. This issue has been addressed here properly via composite and film formation in their pure form without compromising with their

intrinsic properties. Non-covalent interfacial interactions between MoS_2 nanosheets and polymer matrix have been optimised via Langmuir in order to attain the desirable properties of the nanocomposite formed [53,54,58,137].

Herein we have demonstrated the insitu oxidation polymerization of indole monomer in presence of MoS_2 nanosheets (synthesized by green strategy) in aqueous medium. Indole gets adsorbed on MoS_2 nanosheets assisting its exfoliation and these nanosheets in turn act as template for in-situ oxidative polymerization of indole. This work highlights the importance of Langmuir technique in attaining maximum interfacial interaction between MoS_2 nanosheets and PIn at air-water interface. To the best of our knowledge, there is no report available till date on indole assisted exfoliation of MoS_2 nanosheets and their homogenous dispersion via Langmuir method. Our work emphasizes on the simultaneous exploitation of excellent intrinsic properties of both MoS_2 and PIn together via nanocomposite formation to attain desirable large area, thin film via LS method. We believe that this approach describing Langmuir assisted dispersion of 2D materials into polymer matrices (less soluble and lower conductivity) may content the desire to obtain their large-area uniform, compact and stable films for electronic device applications.

5.2 Results and Discussion

5.2.1 Characterization of MoS_2 nanosheets

As observed from TEM micrograph (Figure 5.1 (a)), synthesized MoS_2 reveals nanosheet like structure [135,137,140]. Selected area electron diffraction (SAED) pattern (inset of Figure 5.1 (a) displays ring-like mode confirming their polycrystalline nature. HR-TEM micrograph (Figure 5.1 (b)) was also recorded to get insight of the crystal structure of MoS_2 that clearly shows stacked layers. The interlayer distance (marked in

yellow bars) was measured using Gatan software (Figure 5.1 (c)) and found to be around 0.63 nm from an intensity profile graph [136]. Elemental analysis (Figure 5.1(d)), STEM-HAADF image, elemental mapping image (Figure 5.2) confirm the presence of Mo and S together as MoS_2. X-ray powder diffraction (XRD) pattern (Figure 5.1(e)) of the bulk MoS_2 shows diffraction peaks at 13, 33, 44 and 59° that can be unambigously assigned to (002), (100), (103) and (110) planes of hexagonal phase of MoS_2 (JCPDS No. 37-1492) [136,137,139,142]. The d-spacing observed in Figure 5.1 (b) corresponds to (002) plane which is in good agreement with the present XRD results (Figure 5.1(e)) obtained for MoS_2 and previous reports [139,143]. On the basis of obtained results, we proposed a plausible mechanism (Section 2.2.5.1) that explains the significant catalytic role of H^+ ions in formation of MoS_2 nanosheets. Further, low pH condition also negates the formation of Mo oxides thus favoring the formation of MoS_2 [139].

5.2.2 Interaction studies of MoS_2-PIn nanocomposite

Interactions between the nanosheet and PIn is investigated via UV-Vis and FT-IR spectroscopy. UV-Vis spectra (Figure 5.3) of precursors in pristine form (PIn and MoS_2 nanosheets) and their MoS_2-PIn composite was recorded to investigate the spectral changes after the composite formation. MoS_2 nanosheets exhibited characteristic absorptions at 390, 445, 608 and 660 nm (Figure 5.3 (a) (i) red star marked) which are absent in composite signifying the interaction of nanosheets with PIn.14,24 Figure 5.3 (a) (ii) displayed characteristic absorptions of PIn at 253, 306, 347 (π- π*), 398 nm (n-π*) and polaronic transition (450-550 nm) consistent with reported literatures [51,69,72,119]. These absorptions were consistent with composite (Figure 5.3 (a) (iii)) justifying the polymerization of indole along with 20 nm shift in the first peak (characteristic of indole; blue star marked). This red shift could be attributed to the

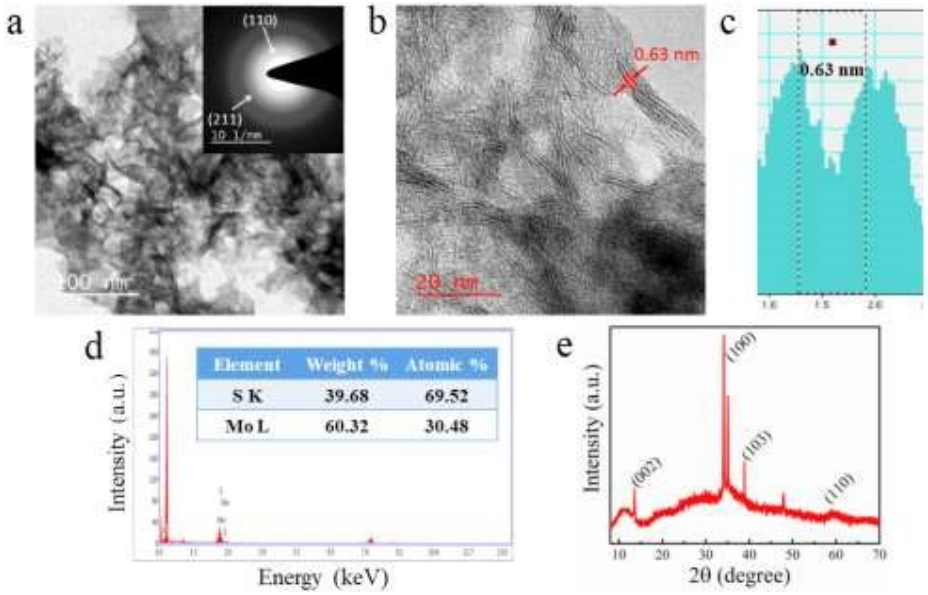

Figure 5.1 Characterizations of MoS_2 nanosheets synthesized via hydrothermal process (a) TEM (inset showing SAED pattern) (b) HRTEM image, (c) intensity profile graph depicting interlayer distance, (d) EDS elemental analysis, (e) XRD pattern.

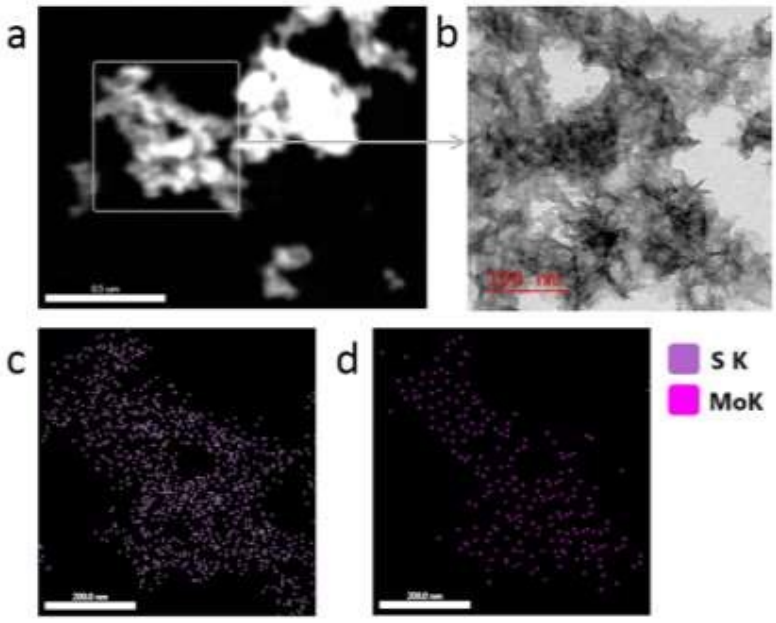

Figure 5.2 (a) HAADF-STEM, (b) TEM image and element mapping images of MoS_2 (c) S, (d) Mo.

increased conjugation length and controlled polymerization of indole on MoS_2 nanosheets [51,72].

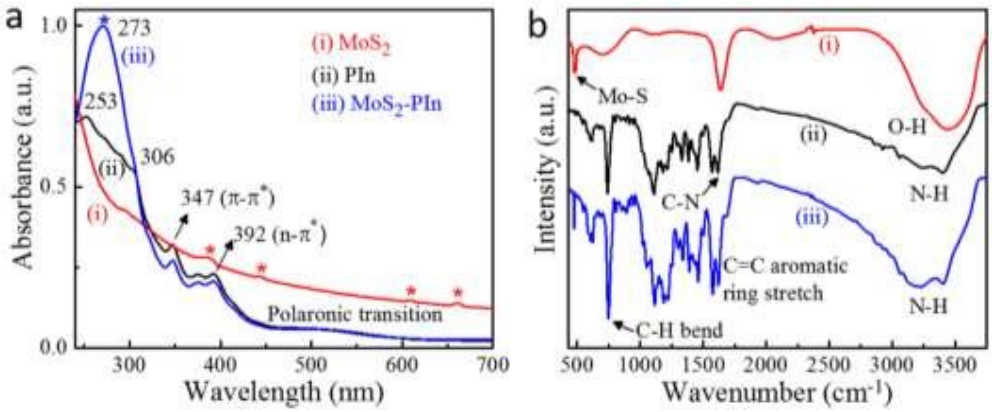

Figure 5.3 (a) UV-vis and (b) vibrational spectroscopy of (i) MoS_2 nanosheets, (ii) PIn and (iii) MoS_2-PIn composite.

FT-IR spectroscopy aided in investigation of the non-covalent interaction between the PIn and MoS_2 nanosheets in their composite. For pure MoS_2 nanosheets (Figure 5.3 (b) (i)), peak at 470 cm^{-1} was assigned to Mo-S stretching vibration and the other two peaks at 1633 and 3434 cm^{-1} correspond to O-H stretching vibrations due to intercalated water molecules [144,145]. Characteristic N-H stretching vibration at 3400 cm^{-1} for PIn and 3403 cm^{-1} for MoS_2-PIn (Figure 5.3 (b) (i) and (ii)) validate 2,3 linkage of monomer unit during polymerization [51,72]. Both Mo-S vibration peak and other characteristic vibration peaks for PIn are consistent in the MoS_2-PIn composite (Table 5.1) along with slight shifts reflecting successfully polymerization of indole onto MoS_2 nanosheets. These red shifts (3-15 cm^{-1}) towards higher wavenumber can be attributed to interaction between the host MoS_2 nanosheet and guest PIn [51,76,137].

XRD pattern of pure PIn and MoS_2-PIn nanocomposite powders are shown in Figure 5.4 (a). Diffraction of pure PIn (Figure 5.4 (a) (ii)) displayed characteristic weak reflections

Table 5.1 Vibrational spectroscopy band assignment of MoS_2, PIn and MoS_2-PIn.

Band assignment (in cm^{-1})	**MoS_2**	**PIn**	**MoS_2-PIn**
Mo-S str	470	-	470
O-H str	1633, 3434	-	-
N-H str	-	3400	3403
N-H bend	-	1616	1621
C=C str (aromatic)	-	1600-1400	1615-1415
C-N str	-	1454	1461
C-H bend	-	741	747

in the range of 15-25° [51,72]. The MoS_2-PIn composite unambiguously showed diffraction peaks corresponding to PIn along with some extra peaks suggesting successful polymerization growth on MoS_2 nanosheets with controlled kinetics. While MoS_2 did not give its signature in composite diffraction pattern. There are two reasons for this: (1) PIn matrix prevented the re-stacking of as-prepared MoS_2 nanosheets (also evident from TEM image Figure 5.5) and (2) MoS_2 is present in very low wt% composition in composite viz. beyond the detection limit of our instrument [142]. This clearly indicates that MoS_2 nanosheets are few atomic layers in the composite.

This MoS_2 guided polymerization of indole in a controlled fashion yielded smaller polymeric fragments as compared to the chemically synthesized pristine PIn. This statement is in support with the FAB mass result that states 5-6 monomer units linked together. This result also confirms that MoS_2 did not affect the PIn diffraction peak positions reflecting that it was not incorporated into the polymer structure, instead it formed non-covalent linkage during polymerization.

Thermal analysis shown in Figure 5.4 (b) clearly distinguishes the degradation temperatures for PIn and MoS_2-PIn composite revealing the improved stability of the nanocomposite synthesized. At marked temperatures (a) 190°C, the weight loss difference was ~4% but at higher temperature (b) 600°C the difference raised to 12% indicating enhancement in thermal stability of the nanocomposite. All the above results validate the existence of non-covalent interaction between the polymerized indole and MoS_2 nanosheet with synergistic enhancement in conjugation length, polymer crystallinity and thermal stability [51,69,72,119,142].

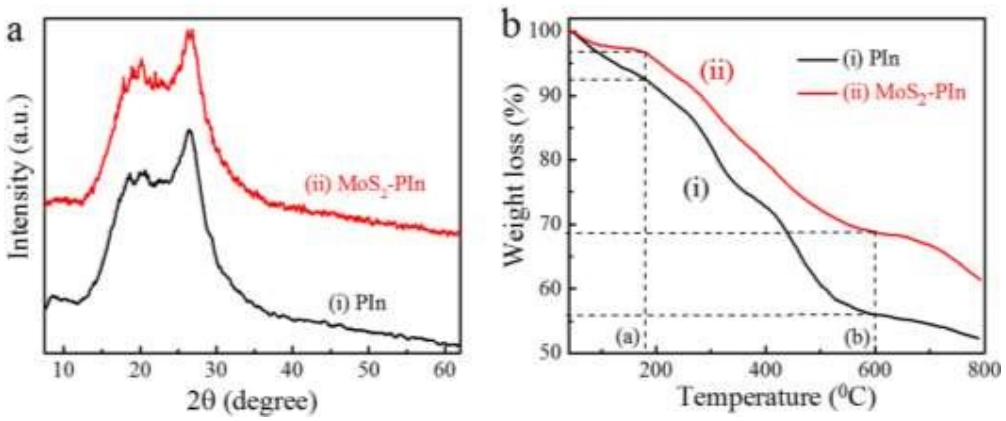

Figure 5.4 (a) XRD pattern and (b) TGA of (i) PIn and (ii) MoS_2-PIn nanocomposite (bulk).

TEM micrographs (Figure 5.5) of in-situ polymerized PIn on MoS_2 as template shows dark black patches representing MoS_2 nanosheets that are embedded onto the lighter backgrounds representing PIn. Figure 5.5 (b) clearly reveals the upper few layers of MoS_2 over the base layer of PIn. STEM image and elemental mapping for the same as shown in Figure 5.6 supports the plausible mechanism (Figure 2.4) of homogenous growth of PIn over nanosheets [142]. The image (Figure 5.6) clearly corresponds to differents elements such as Mo, S, C and N uniformly distributed over the patched area.

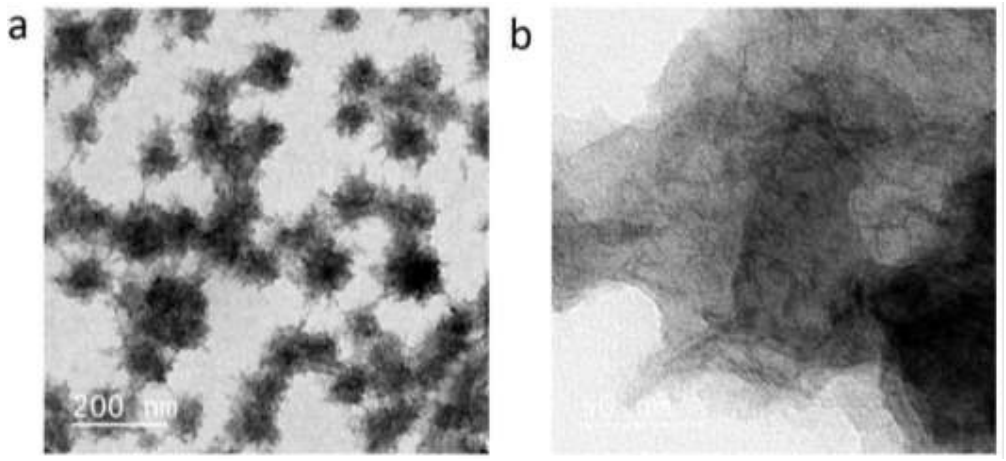

Figure 5.5 TEM micrographs of drop casted MoS_2-PIn nanocomposite at different scale bars (a) 200 nm **(**b) 50 nm.

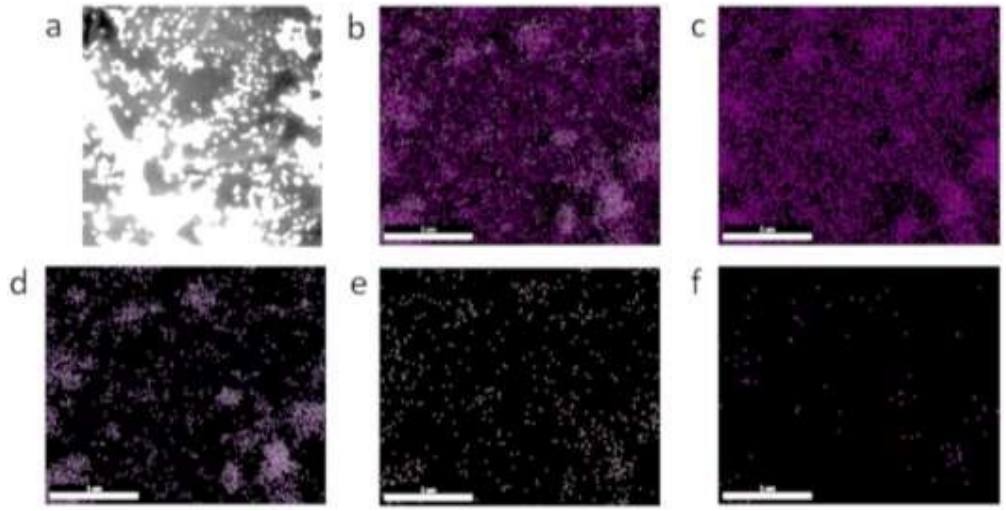

Figure 5.6 (a) HAADF-STEM and (b) element mapping images of MoS_2-PIn nanocomposite (bulk drop casted): (c) C, (d) N, (e) S, (f) Mo.

MoS_2 concentrations in increasing order namely MoS_2-PIn-1, MoS_2-PIn-2 and MoS_2-PIn-3 were also employed for nanocomposite formation and optimized using CV and TEM measurements. Cyclic voltammograms for pure PIn, MoS_2 and various MoS_2-PIn-1,2,3 combinations were obtained in a 5 mM $[Fe(CN)_6]^{3-/4-}$ mixture (1:1); 0.1 M KCl (see

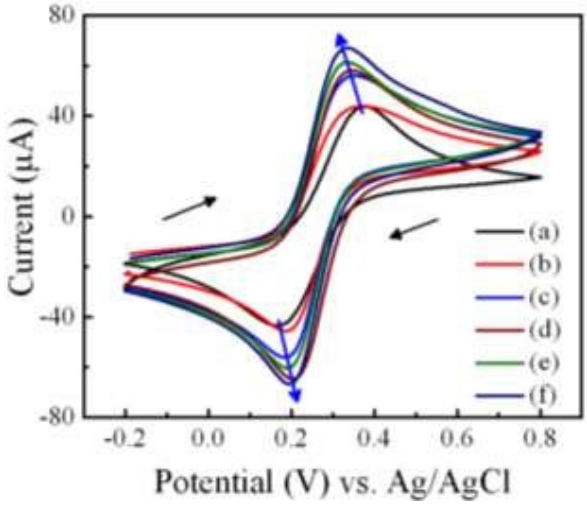

Figure 5.7 CV curves of (a) GCE, (b) MoS_2/GCE, (c) PIn/GCE, (d) MoS_2-PIn-1/GCE, and (e) MoS_2-PIn-2/GCE (f) MoS_2-PIn-3/GCE in a 5 mM $[Fe(CN)_6]^{3-/4-}$ mixture (1:1); 0.1 M KCl (Scan rate 20 mVs^{-1}).

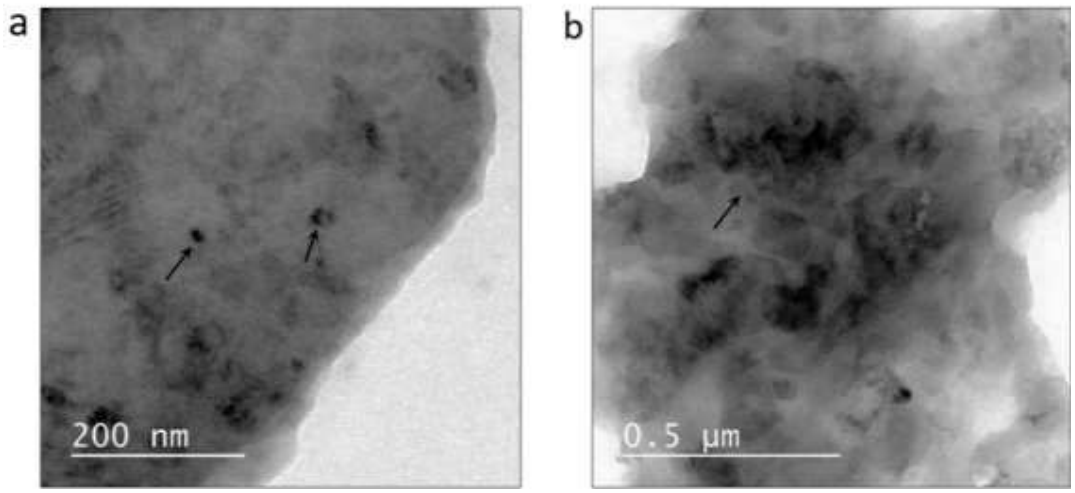

Figure 5.8 TEM micrographs of LS films of (a) MoS_2-PIn-1 and (b) MoS_2-PIn-3 (dark patches pointed with arrows represent MoS_2).

Figure 5.7). This clearly illustrates the enhancement in both anodic and cathodic peak current upto highest composition MoS_2/PIn-3 and decrease in potential separation (peak to peak) as compared to pure PIn and MoS_2. This can be attributed to the synergistic

effect between the components of nanocomposite leading to increment in conductivity [135,146]. TEM images of the above two compositions (1 and 3) reveal very low dispersion of nanosheets in PIn matrix (see Figure 5.8 (a)) for 1, whereas aggregation of MoS_2 (see Figure 5.8 (b)) in the highest composition MoS_2/PIn-3 (dark patches marked with arrow represent MoS_2). Hence, MoS_2-PIn-2 composition representing well grown PIn over MoS_2 nanosheets (Figure 5.5) consented by TEM and CV studies together, is the optimum one to carry on other studies.

On the basis of above results, we proposed a schematic (shown in Figure 2.4) describing MoS_2 nanosheet synthesis via facile hydrothermal method, addition of indole to the MoS_2 nanosheets followed by ultrasonication. Herein, ultrasonication in an ethanol/aqueous mixture in presence of indole facilitated adsorption of indole unit onto nanosheets coordinating to the metal chalcogenide center via nitrogen. This aqueous dispersion when subjected to APS (oxidant), assisted in controlled and assembled synthesis of PIn particles on MoS_2 nanosheets serving as template. Once the polymer was formed, it directed the orientation of nanosheets. Monomers adsorbed on template, prior to polymerization results in controlled and ordered polymer formation playing significant role in solution processability [18,59,76,147].

5.2.3 Floating film isotherm studies

Molecular interaction at air-water interface was investigated via pressure-area (π-A) isotherm study (Figure 5.9) of PIn and MoS_2-PIn composite in LB trough. Various parameters that determine the film properties were optimized according to our previous reports [55,63,76]. Also, it was observed that vertical lifting of the PIn LB film, decrement of transfer ratio for multilayer was observed [53,54,76]. This was probably

due to reverting back of the film into subphase during vertical upliftment. So, horizontal or LS method of film lifting especially for non-amphiphilic molecules is highly preferrable to obtain good quality films [53,54,76]. Chemically synthesized PIn and MoS_2-PIn were taken in very dilute concentration (~1.0 mg/mL) for spreading over langmuir trough. Figure 5.10 very well depicts the process of self-assembly of MoS_2-PIn initially and after barrier compression at the rate of 10 mm/min. On compression, the floating film islands of composite start arranging themselves to form continous film. Pressure-area (π-A) isotherm of both PIn and MoS_2-PIn in Figure 5.9 (a) and (b) illustrates the effect of increasing surface pressure on mean monomeric area of the sample. Both isotherms have been sub-divided into four distinct regions as per our earlier reports marked as region I for gaseous phase (molecules far apart) reflecting weak intermolecular interactions, II for liquid condensed phase, III for solid condensed and IV for solid collapse phase (monolayers start collapsing) [55,63,76]. As evident from Figure 5.9, mean monomeric area for (b) MoS_2-PIn is larger than that for (a) PIn that can be attributed to the MoS_2 nanosheets forming strong secondary interactions with PIn occupying larger surface coverage alongwith reduction in film rigidity. Chain extension of PIn anchored on MoS_2 nanosheet occurs widely over the subphase giving rise to monolayer and uniform film. Being non-amphiphilic, PIn alone forms pseudomonolayer (thicker layer) which is evident from AFM results discussed later [76,135,137]. Moreover, higher collapse point for the MoS_2-PIn isotherm also demonstrates relative better monolayer stability at air-water interface than PIn. Blodgett style (vertical deposition) film lifting leads to aggregate and discontinous film formation especially in the case of multilayer deposition [53,147]. This was consistent with our observations of diminishing transfer ratio from 0.95 to 0.45 for multilayer deposition as observed in Table

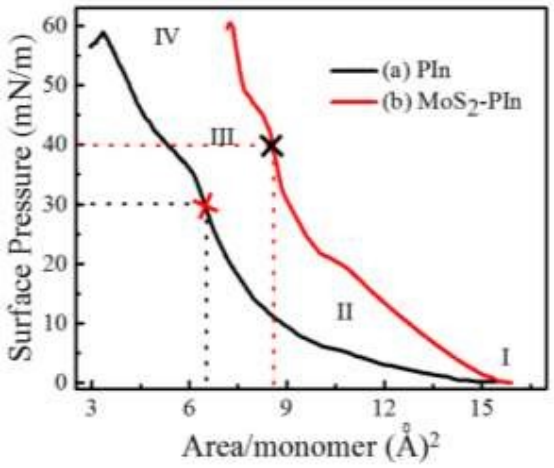

Figure 5.9 Pressure vs. Area (π-A) isotherm of (a) PIn and (b) MoS_2-PIn nanocomposite.

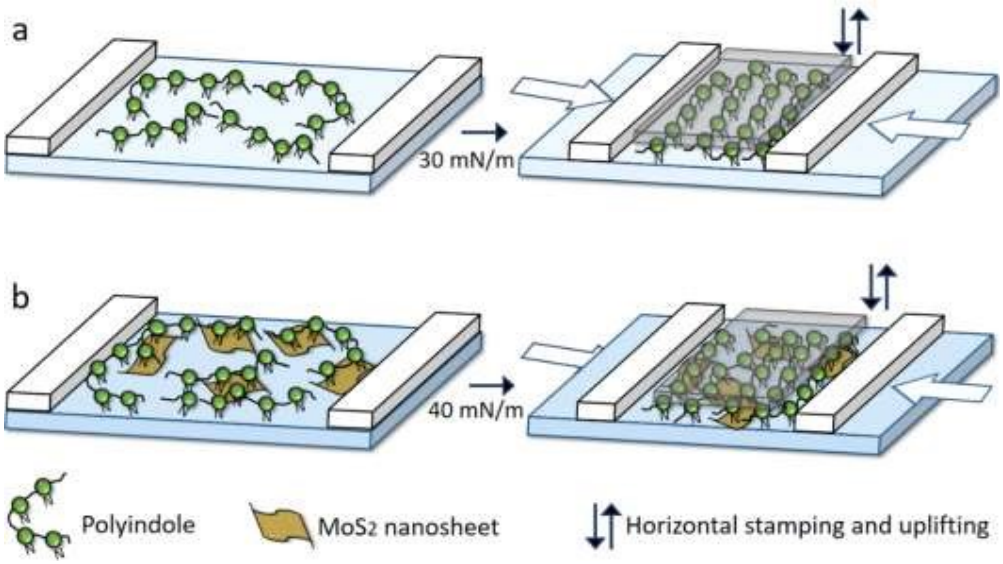

Figure 5.10 Schematic representation of assembly of MoS_2-PIn on water subphase initially, after barrier compression and LS film fabrication.

5.2. Moreover, there is risk of monolayer to revert back into the subphase during vertical lifting. Therefore, for non-amphiphilic molecules like PIn, LS technique is more preferable. The substrate is stamped horizontally and lifted very slowly (manually) making an angle of 45° with the subphase. This is referred as semi-dry process as the

substrate lifting doesnot directly disrupt the Langmuir monolayer unlike vertical uplifting.

Table 5.2 Transfer ratio of different number of layers (I, III, V) deposited.

Material	**Surface Pressure (mN/m)**	**Transfer ratio (n) for different layers**					
		Vertical dipping (LB)			**Horizontal dipping (LS)**		
		I	**III**	**V**	**I**	**III**	**V**
PIn	30	0.95	0.84	0.43	1.5	0.95	0.85
MoS_2-PIn	40	0.95	0.65	0.40	1.0	0.95	0.84

5.2.4 Topographical and structural analysis of LS films

TEM and AFM studies were performed to investigate the uniform dispersion of MoS_2 nanosheets in PIn matrix. TEM micrographs (Figure 5.11 (a) and (b)) of PIn LS film shows its expanded sheet like structure wrinkled at places probably due to lifting flaws on carbon grid. TEM image (Figure 5.11 (c) and (d)) of MoS_2-PIn LS films clearly exhibit MoS_2 nanosheets (dark patches) decorated uniformly in PIn matrix. These nanosheets are uniform in size ranging from 40-60 nm diameter decorated uniformly. Percentage of surface area coverage of MoS_2 nanosheets on PIn LS film as calculated via ImageJ from Figure 5.11 (d) was found to be 20±3 %. Moreover, STEM image and elemental mapping of the MoS_2-PIn LS films (see Figure 5.12) also validated the dark patches as MoS_2 nanosheets on PIn matrix. Surface topography images of PIn and MoS_2-PIn LS films were investigated along with Phase contrast images simultaneously as shown in Figure 5.13 (a-d). AFM images of PIn LS films (Figure 5.13 (a)) reveal the uniformity and compactness with average height profile of ~4.5 nm similar to our previous report.35 Average height profile of nanocomposite comes to be ~ 3.5 nm which suggest the

formation of well dispersed three or fewer layers of MoS_2 on PIn matrix. This finding also complements the larger mean monomeric area observed for composite (Figure 5.9 (b)). Moreover, nanocomposite forms more uniform and smooth film as compared to pure polymer that is clearly evident from rms roughness values of 0.895 nm in comparison to 0.200 nm obtained for PIn. The difference in topography from previously reported work on PIn can be attributed to different lifting method of Langmuir films and different synthetic route for polymerization of indole [76]. Phase contrast image (Figure 5.13 (b)) of PIn LS film doesnot reveal much information except the same composition throughout. AFM image of MoS_2-PIn nanocomposite LS films (Figure 5.13 (c)) shows white patches of uniform size homogenously distributed over the matrix. The same could be observed in its phase contrast image (Figure 5.13 (d)). Phase contrast images sensitive to compositional difference, very well depict the presence of two phases in nanocomposite. This observance strongly supports the TEM result (Figure 5.11 (c) and (d)) signifying homogenous distribution of uniform sized MoS_2 nanosheet on PIn matrix facilitated by Langmuir method self-assembly.

5.2.5 Electrical Characterization

The charge transport properties and electronic parameters of layer by layer deposited PIn LS film was investigated from sandwiched structure of Al/PIn/ITO and Al/PIn-MoS_2/ITO [56,59,67,68,147]. Figure 5.14 (a) shows the J-V characteristics of PIn LS film and PIn-MoS_2 LS film respectively. However, Figure 5.14 (b) demonstrate the semi-log plot of Figure 5.14 (a) under dark condition at room temperature. The fabricated sandwiched structure fabricated device ITO/Semiconductor/Al Schottky junction is shown in the schematic diagram (inset of Figure 5.14 (a)). The rectifying behavior of the sandwiched structure devices were evaluated by assuming the standard thermionic

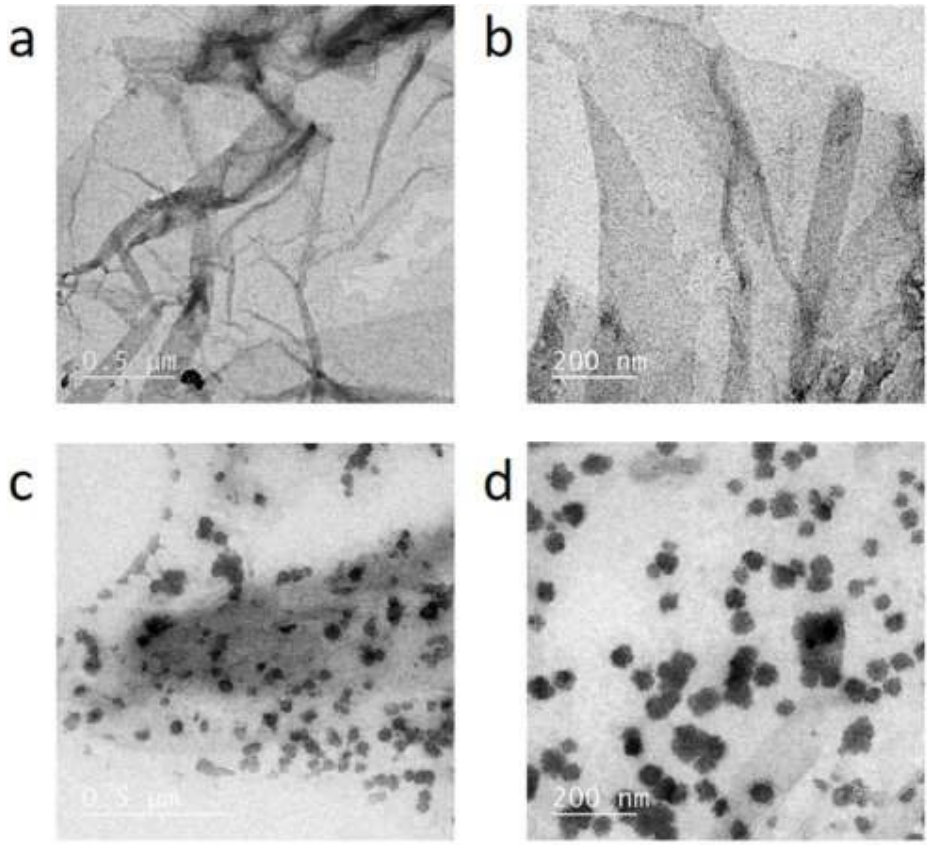

Figure 5.11 TEM micrographs of LS films of (a,b) PIn and (c,d) MoS_2-PIn.

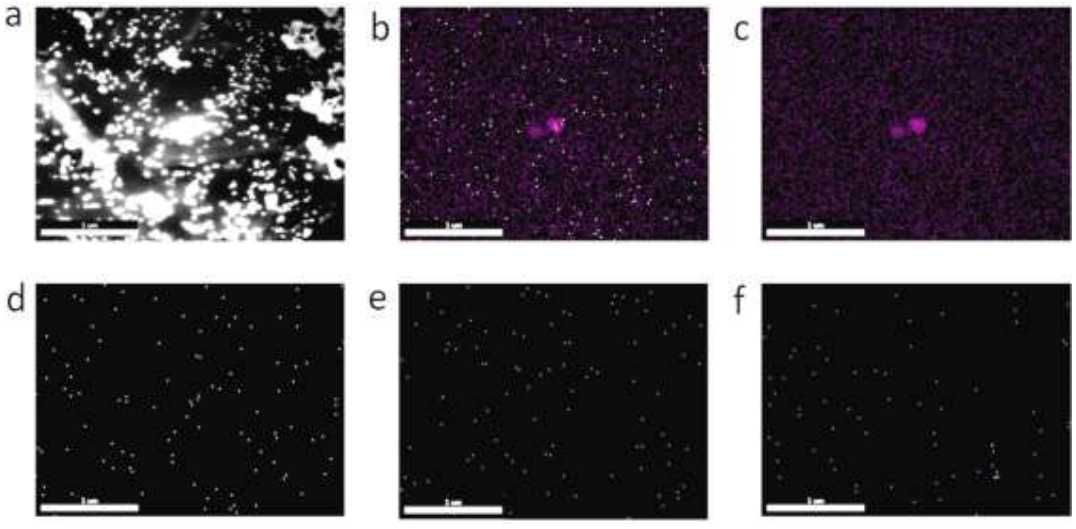

Figure 5.12 (a) HAADF-STEM and (b) element mapping images of MoS_2-PIn LS film: (c) C, (d) N, (e) S, (f) Mo.

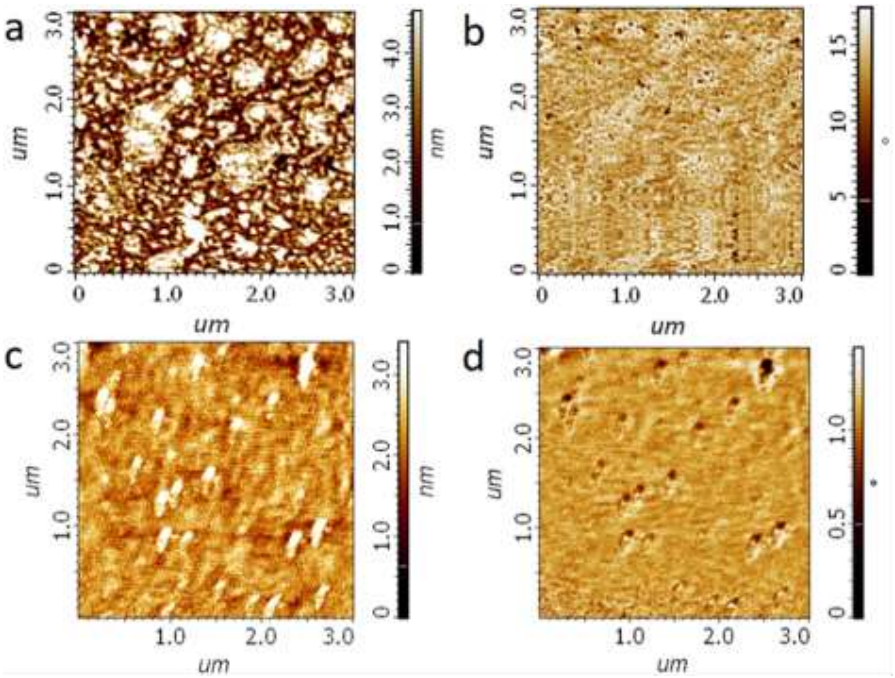

Figure 5.13 Tapping mode AFM and phase contrast images of LS films of (a,b) PIn and (c,d) MoS_2-PIn.

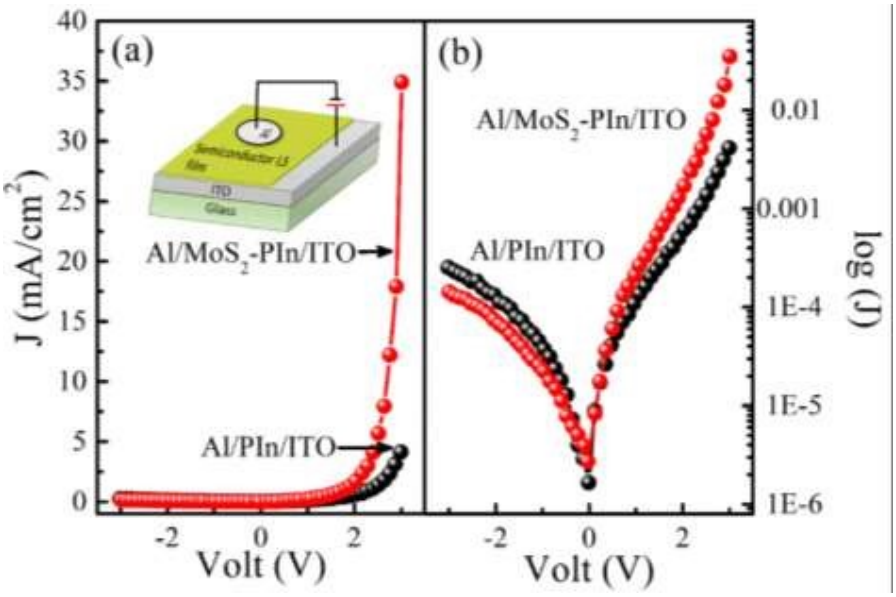

Figure 5.14 (a) Current density-voltage (J-V) measurement (b) Semi-log plot for 5 layered LS film fabricated Al/PIn/ITO (black curve) and Al/ MoS_2-PIn/ITO (red curve) device structure.

emission theory which can be expressed as [56,59]

$$J = J_0\left(exp\left(\frac{qV}{\eta kT}\right) - 1\right) \qquad (5.1)$$

$$\eta = \frac{q\Delta V}{kT\Delta lnJ} \qquad (5.2)$$

Where J_0 denotes the saturation current density in absence of external bias, η is the ideality factor of device, q is electronic charge, and V is the applied voltage, T is temperature in Kelvin and k is the Boltzmann constant. J_0 is associated with the Schottky barrier height, Φ_B as

$$J_0 = A^*T^2 \exp\left(\frac{-q\Phi_B}{kT}\right) \qquad (5.3)$$

$$\Phi_B = \frac{-q}{kT}\ln\left(\frac{J_0}{A^*T^2}\right) \qquad (5.4)$$

Where A* is the effective Richardson constant (value=120 A cm^{-2} K^{-2}). Based on the above equations, we calculated the saturation current density J_0, barrier height Φ_B and ideality factor η of devices Al/PIn/ITO and Al/PIn-MoS_2/ITO given in Table 5.3. The ideality factor of Al/PIn/ITO device demonstrates deviation from ideal diode behaviour and much higher value in comparison to ideal diode ideality factor (=1). However, the ideality factor of both devices viz Al/PIn/ITO and Al/PIn-MoS_2 is larger than one. It is

Table 5.3 Electronic parameters of device.

Parameter→ Devices ↓	**η**	**J_0 (A/cm^2)**	**Φ_B (eV)**	**Rectification ratio**
Al/PIn/ITO	4.55	1.15x10^{-6}	0.684	22
Al/MoS_2-PIn/ITO	3.54	1.45x10^{-6}	0.676	240

important to note that the ideality factor between 1.0 and 2.0 arises due to carrier drift diffusion process and the Sah-Noyce-Shockley generation recombination process. There are several phenomena that can attribute to the exceeding value of ideality factor such as trap-assisted tunneling, carrier leakage, and barrier inhomogeneity, etc. Therefore, ideality factor more than 2 in both case LS films is due to layer by layer deposition (upto five layers) causing increase in trap-assisted tunneling, carrier leakage, and barrier inhomogeneity. Multilayer deposited PIn LS films devices with the deviation from ideal behavior is consistent with our previous assumptions [59,147]. However, addition of MoS_2 nanosheets in polymer film matrix induces betterment in the ideality factor from 4.55 to 3.54.

The current obtained for Al/MoS_2-PIn/ITO devices demonstrate significantly ~9 fold enhancement in forward current as compared to pure Al/PIn/ITO. This enhancement in forward current can be explained by using Mott's law of variable-range hopping for variety of disordered materials. It is noteworthy, that three type of conduction pathways are possible in the MoS_2-PIn materials. First one, along the conjugation length of polymer chains; second one, hopping between the polymer chains and third one, conduction via MoS_2 conducting filler. This conducting filler plays a vital role in this remarkable enhancement in conductivity because fillers provide an easy path for charge conduction. It means nanofiller MoS_2 contributes remarkably towards the significant enhancement in current. Further, addition of MoS_2 nanofillers cause improvement in saturation current and successive reduction in barrier height from 0.683 to 0.676 as shown in Table 5.3.

Finally, it is noteworthy to mention that the MoS_2-PIn LS film demonstrated 10 fold enhancement in rectification ratio as compared to pure PIn LS film. The remarkable

increment in rectification ratio can be attributed to the formation of smooth surface, reduction in barrier height and enhancement in charge injection efficiency.

5.3 Conclusion

MoS_2 nanostructures successfully synthesized via hydrothermal reaction that yielded its nanosheet morphology, guided the controlled growth of PIn. The non-covalent interaction between MoS_2 nanosheet and nitrogen atom of indole unit was the driving force of exfoliation in aqueous medium and assembly at air-water interface. These pre-assembled structures were tailored using Langmuir technique for large area uniform dispersion of MoS_2 nanosheets on PIn matrix. This hypothesis was validated by TEM and AFM results. LS technique offered remarkable opportunity to nanocomposite to self-assemble and disperse themselves at the air-water interface. MoS_2 nanosheets formed larger interface with higher surface to mass ratio on PIn matrix in Langmuir trough leading to stable and uniform film. Furthermore, this simple approach for homogenous distribution of uniform sized MoS_2 nanosheets in PIn matrix exhibited significant enhancement in electrical properties of the polymer. We hope that this work will encourage the usage of Langmuir technique for obtaining homogenously dispersed 2D materials in other polymer matrices too.